Wavelets for Agriculture and Biology: A Tutorial with Applications and Outlook

XUEJUN DONG, PAUL NYREN, BOB PATTON, ANNE NYREN, JIM RICHARDSON, AND THOMAS MARESCA

Wavelet transforms (WTs) are finding increasing use in the discovery of the scale-specific properties of complex biological data. Although many efforts have been made to explain the main concepts of WT without advanced mathematics, the implicit reliance on digital signal processing terminology is widespread in many popular articles. This may cause some confusion for many biologists who do not have a clear understanding of the computational mechanisms and computer graphics of WTs. In this article we provide a tutorial on WTs for biologists by walking through two carefully selected examples step-by-step, using freely available software as well as a self-developed computer program. Both discrete WT and continuous WT are discussed, and detailed computational instructions, along with thorough interpretations of the computer outputs (or hand-calculated steps), are provided throughout. We conclude by offering a few directions for further study and several ideas on possible new developments in biological sciences using wavelets.

Keywords: biological information, computer application, interdisciplinary research, long-term weather data, multiresolution analysis

**In recent years, wavelet transforms (WTs), as originally developed in the 1980s (Hubbard 1998), are finding increasing use in biological and related sciences, including studies on climate patterns (Lau and Weng 1995), biological community dynamics (Keitt and Fischer 2006), ecological patterns and scales (Dale and Mah 1998, Lark and Webster 1999, Keitt 2000, Csillag and Kabos 2002, Keitt and Urban 2005, Mi et al. 2005), forest gap structure (Bradshaw and Spies 1992), landscape remote sensing (Strand et al. 2006), biomolecules (Lió 2003, Haimovich et al. 2006), bird sounds (Selin et al. 2007), and human brain signals (Keil et al. 2003). In particular, wavelet multiresolution analysis (MRA) enables one to visualize the structures buried in different time (spatial) scales just as one would see the subcellular structures of living things using a microscope (Hubbard 1998, Walker 1999). Although works by Hubbard (1998), Walker (1999), Jensen and Cour-Harbo (2000), Polikar (2001), and Fugal (2007) have explained the concepts of WT without relying on advanced mathematics, and many wavelet computer programs (e.g., Fawave, and routines with Matlab, R, and S-plus) are now readily available, the implicit assumption in these explanations is that the reader is familiar with the terms of digital signal processing (DSP), an assumption that may be inaccurate for some biological and applied scientists. Moreover, most articles are rich in output graphics but deficient when it comes to detailed interpretations, which may leave biologists puzzled about how the WTs were generated. In addition, effective communication among biologists from different research areas seems limited, despite the fact that they all may be using the same WT technique to tackle complex problems in their respective fields.

We have two objectives in this article. First, we hope to provide a practical tutorial so that biologists can quickly understand the basic idea of WT without extensive knowledge of DSP and advanced mathematics. This will be accomplished by walking through two carefully selected examples step-by-step, using freely available software. We also provide detailed computational instructions and a thorough interpretation of the results. Second, we offer a few brief but critical comments for further study of the wavelet technique, and we highlight a few research topics that are advancing rapidly or are likely to stimulate new thoughts in biological sciences.

Data source and analysis methods

Our sample data set includes an eight-element artificial "signal" (Jensen and Cour-Harbo 2000) and monthly Palmer Drought Severity Index (PDSI) data from 1921 to 2006 for

Xuejun Dong (e-mail: xuejun.dong@ndsu.edu) and Bob Patton are assistant range scientists, Paul Nyren is a range scientist, and Anne Nyren is an administrative officer and Web master at North Dakota State University, Central Grasslands Research Extension Center, Streeter, North Dakota. Jim Richardson is a professor emeritus with the Department of Soil Sciences at North Dakota State University in Fargo. Thomas Maresca is a retired electrical engineer from Philadelphia.

the nine climate regions of North Dakota, United States (NESDIS 2006). The physical locations of the climate divisions for North Dakota are northwest, north-central, northeast, west-central, central, east-central, southwest, south-central, and southeast (LUSCD 2007). The PDSI values generally range from –6 to +6, with negative values denoting dry spells and positive ones for wet spells. Both discrete WT (DWT) (Walker 1999) and continuous WT (CWT) (Polikar 2001) were used for analyzing the PDSI data. Data analysis was conducted with MINITAB and WTs using the free software TimeStat (*www.pricepatternprediction.com/ga01011.htm*), FracLab (*http://complex.futurs.inria.fr/FracLab/download.html*), and Fawave (*www.uwec.edu/walkerjs/*). Although we used only the outputs from TimeStat and FracLab, we verified most of the results with Fawave as well as with a computer program of our own.

The essential idea of wavelet multiresolution analysis

Many complex natural signals, such as a time series of soil electrical conductivity (Lark and Webster 1999) or an aerial image of a landscape-scale vegetation map (Strand et al. 2006), have small variations at fine scales and large ones at coarse scales. The MRA, "the heart of wavelet analysis" (Walker 1999), can be used to successively break down these kind of signals into several pieces, each representing a different scale. Using WT, these simpler component signals can be manipulated in various ways with high flexibility before they are synthesized to achieve different signal processing and enhancement objectives (Fugal 2007). For example, some components may be discarded because of their small magnitude and thus small contribution to the total energy (or variance in biology) of the whole signal (Shapiro 1993). This may lead to noise removal, image enhancement (Shapiro 1993, Walker and Chen 2000), and breakdown of autocorrelation (Keitt 2000, Lió 2003). In the next two sections, we show detailed calculations of WTs using a sample data set. We encourage readers to use a pencil and paper to work through the calculations for the eight-element signal. After this, one may analogize to understand the PDSI data analysis.

Discrete wavelet transform using an artificial signal

Conventional DWT decomposes the original signal successively into components of different scales by powers of 2 (Fugal 2007), first splitting the original signal in halves, then in quarters, and so on. We will use an eight-element signal, $f = (56,40,8,24,48,48,40,16)$, to illustrate its essence. First, for ease of discussion, we review several terms used by Walker (1999). Let this signal be $f = (f_1, f_2, ..., f_8)$, and the first trend subsignal $a1 = (a_1^1 = 48, a_2^1 = 16, a_3^1 = 48, a_4^1 = 28)$, in which a_i^1 is obtained by

$$a_i^1 = \frac{f_{2i-1} + f_{2i}}{2}, \qquad (1)$$

where $i = 1,2,3,4$. Let the first fluctuation subsignal be $d1 = (d_1^1 = 8, d_2^1 = -8, d_3^1 = 0, d_4^1 = 12)$, in which d_i^1 is obtained by

$$d_i^1 = \frac{f_{2i-1} - f_{2i}}{2}, \qquad (2)$$

where $i = 1,2,3,4$. We start from f and obtain the first trend subsignal $a1$ and the first fluctuation subsignal $d1$, where the length of each of the latter two subsignals is half that of the original signal. By working on $a1$, equations 1 and 2 can be applied recursively to obtain the second trend subsignal $a2$ and second fluctuation subsignal $d2$. As we proceed one more recursive step, we find $a3$ and $d3$, as shown in box 1 (Jensen and Cour-Harbo 2000).

Box 1. A 3-level decomposition of the original signal,

Original signal	$\underbrace{56,40,8,24,48,40,16}_{f}$
First decomposition	$\underbrace{48,16,48,28}_{a1},\underbrace{8,-8,0,12}_{d1}$
Second decomposition	$\underbrace{32,38}_{a2},\underbrace{16,10}_{d2},\underbrace{8,-8,0,12}_{d1}$
Third decomposition	$\underbrace{35}_{a3},\underbrace{-3}_{d3},\underbrace{16,10}_{d2},\underbrace{8,-8,0,12}_{d1}$

Reconstruction. Now we perform a perfect reconstruction of the original signal f, beginning from $a3$. Because $a3$ and $d3$ are obtained solely from $a2$ (i.e., $a_1^3 = \frac{a_1^2 + a_2^2}{2} = \frac{32+38}{2} = 35$ and $d_1^3 = \frac{a_1^2 - a_2^2}{2} = \frac{32-38}{2} = -3$), to reconstruct $a2 = (a_1^2, a_2^2)$ we need to do some simple algebra. To find a_1^2, we add the two equations in parentheses, that is, $a_1^3 + d_1^3 = \frac{a_1^2 + a_2^2}{2} + \frac{a_1^2 - a_2^2}{2} = a_2^2$, and thus $a_1^2 = a_1^3 + d_1^3 = 35 + (-3) = 32$ Similarly, to find a_2^2, we subtract the two equations in parentheses, that is, $a_1^3 - d_1^3 = \frac{a_1^2 + a_2^2}{2} - \frac{a_1^2 - a_2^2}{2} = a_2^2$, and thus, $a_2^2 = a_1^3 - d_1^3 = 35 - (-3) = 38$ (box 1). Continuing this procedure, we find $a1$ based on $a2$ and $d2$, and finally f based on $a1$ and $d1$, which is a perfect reconstruction. If we make a minor modification by setting only the element $d3$ to zero, that is, $d3 = 0$, and do the reconstruction again, we will get the synthesized signal $f = (59,43,11,27,45,45,37,13)$. This is called an *imperfect reconstruction*—this synthesized signal is different from the original signal f (box 1). However, the error is relatively small because –3 is relatively a small number (compared with most of the other nonzero elements) in this sample signal.

The first averaged and detail signals through reconstruction. Let's look at the first step of decomposition of the original signal *f*. If we set all the elements of *d*1 to zero, *d*1 = (0,0,0,0), and reconstruct *f* from *a*1 and *d*1 using the same rule as we used above, we obtain a signal that is less variable than *f* but still retains the main trend. This is called the *first averaged signal, A*1 = (48,48,16,16,48,48,28,28), because the first fluctuation subsignal *d*1 is totally ignored in the reconstruction, and the synthesized signal *A*1 contains only the contribution from the first trend subsignal *a*1. Compared with *f, A*1 has a lower resolution: the original resolution contains all the details of the signal, but the lower resolution *A*1 does not contain the *first fluctuation subsignal.* By doing this, we have used a "low pass filter" to process the signal (by blocking the rapidly changing components while allowing the slowly changing components to pass through). Similarly, we can set all the elements of *a*1 to zero, that is, *a*1 = (0,0,0,0), while keeping *d*1 unchanged that is, *d*1 = (8,–8,0,12), and do the reconstruction. This will result in the first detail signal, *D*1 = (8,–8,–8,8,0,0,12,–12), because only the information of the fluctuation *d*1 is retained in the reconstruction. By doing this, we have used a "high pass filter" to process the signal (by blocking the slowly changing components while allowing the rapidly changing components to pass through). This is MRA.

Averaged and detail signals for more levels. Using the same procedure as the one for obtaining *A*1 and *D*1, we can find *A*2 (the second averaged signal) and *D*2 (the second detail signal). To find *A*2, we start from *a*2 = (32,38) and *d*2 = (0,0) and reconstruct the new *a*1 as *a*1 = (32,32,38,38). Then we use *d*1 (0,0,0,0) and the new *a*1 (32,32,38,38) to reconstruct the "original" signal (now called *A*2 because during the reconstruction only the information of *a*2 was retained): *A*2 = (32,32,32,32,38,38,38,38). *D*2 can be obtained by setting *a*2 = (0,0), *d*2 = (16,10), and *d*1 = (0,0,0,0) and using the same rule to reconstruct the new original signal. Similarly, we can find *A*3 (the third averaged signal) and *D*3 (the third detail signal). We list them all below, along with the original signal:

$$\begin{aligned} f &= (56, 40, 8, 24, 48, 48, 40, 16)\\ A1 &= (48, 48, 16, 16, 48, 48, 28, 28)\\ A2 &= (32, 32, 32, 32, 38, 38, 38, 38)\\ A3 &= (35, 35, 35, 35, 35, 35, 35, 35)\\ D1 &= (8, -8, -8, 8, 0, 0, 12, -12)\\ D2 &= (16, 16, -16, -16, 10, 10, -10, -10)\\ D3 &= (-3, -3, -3, -3, 3, 3, 3, 3). \end{aligned}$$

Walker (1999) defined the addition of two signals, $g = (g_1, g_2, g_3, g_4)$ and $h = (h_1, h_2, h_3, h_4)$, as

$$g + h = (g_1 + h_1, g_2 + h_2, g_3 + h_3, g_4 + h_4). \quad (3)$$

The original signal *f* can be expressed as the addition of the average and detail of different levels, as shown below (verifiable using equation 3):

$$\begin{aligned} f &= A1 + D1\\ &= A2 + D2 + D1\\ &= A3 + D3 + D2 + D1. \end{aligned}$$

The representation of the relationships among the components of the original signal enables a flexible decomposition or synthesis of the signal, which will be discussed in more detail in the next section.

Wavelets and scaling functions. How are the decomposition and reconstruction of our eight-element signal related to wavelets? One of the simplest wavelets, the Haar, is defined as $H = \left(\frac{1}{\sqrt{2}}, -\frac{1}{\sqrt{2}}, 0, 0, 0, 0, 0, 0\right)$ (Walker 1999), assuming eight elements. It is called "wavelet" because all the elements are zero except the first two, showing a "little wave." To simplify hand calculation, we modify the Haar wavelet so that it reads $x = \left(\frac{1}{2}, -\frac{1}{2}, 0, 0, 0, 0, 0, 0\right)$. It is possible for the nonzero values of *X* to be shifted to give three variations, for example, $X1 = \left(0, 0, \frac{1}{2}, -\frac{1}{2}, 0, 0, 0, 0\right)$ $X2 = \left(0, 0, 0, 0, \frac{1}{2}, -\frac{1}{2}, 0, 0\right)$ $X3 = \left(0, 0, 0, 0, 0, 0, \frac{1}{2}, -\frac{1}{2}\right)$ (figure 1). We will show that the first fluctuation subsignal *d*1 can be expressed as a function of *X, X*1, *X*2, and *X*3. To do this, we first borrow from Walker (1999) the definition of "element-by-element product" of two signals $g = (g_1, g_2, g_3, g_4)$ and $h = (h_1, h_2, h_3, h_4)$ as

$$g \cdot h = g_1 h_1 + g_2, h_2 + g_3 h_3 + g_4, h_4. \quad (4)$$

The first fluctuation subsignal *d*1 can be expressed as *d*1 = $(X \cdot f, X1 \cdot f, X2 \cdot f, X3 \cdot f)$ (figure 1). To verify this, we see that the first element of *d*1 is $\frac{f_1 - f_2}{2} = \left(\frac{1}{2}, -\frac{1}{2}, 0, 0, 0, 0, 0, 0\right) \cdot (f_1, f_2, f_3, f_4, f_5, f_6, f_7, f_8) = X \cdot f$ according to equations 2 and 4. In other words, using equation 2 to calculate the first element of *d*1 is equivalent to using the product of the original signal *f* and the wavelet *X*.

Similarly, we can verify $d_2^1 = X1 \cdot f$, $d_3^1 = X2 \cdot f$, and $d_4^1 = X3 \cdot f$. For the same reason, the first trend subsignal $a1$ can be expressed as $a1 = (Y \cdot f, Y1 \cdot f, \cdot Y2 \cdot f, Y3 \cdot f)$, where Y, $Y1$, $Y2$, and $Y3$ represent the scaling function and its shifts, that is, $Y = \left(\frac{1}{2},\frac{1}{2},0,0,0,0,0,0\right)$, $Y1 = \left(0,0,\frac{1}{2},\frac{1}{2},0,0,0,0\right)$, $Y2 = \left(0,0,0,0,\frac{1}{2},\frac{1}{2},0,0\right)$, $Y3 = \left(0,0,0,0,0,0,\frac{1}{2},\frac{1}{2}\right)$ (figure 1).

To go to the second-level decomposition of f, we use $d2 = (X^{(2)} \cdot a1, X1^{(2)} \cdot a1)$ and $a2 = (Y^{(2)} \cdot a1, Y1^{(2)} \cdot a1)$, where the size of $X^{(2)}$, $X1^{(2)}$, and so on, is each trimmed by the power of 2 with $X^{(2)} = \left(\frac{1}{2},\frac{1}{2},0,0\right)$, $X1^{(2)} = \left(0,0,\frac{1}{2},\frac{1}{2}\right)$, and so on.

The same is true for all other levels of decomposition. As the trend signals shrink through decomposition (box 1), each element contains the information of a wide spatial (time) interval of the original signal. In sum, the signal decomposition using the modified Haar wavelet is easily understood by realizing that it proceeds iteratively with equations 1 and 2 applied to all levels, and with decomposition occurring only on the original or the trend subsignals. As the signal shrinks, the wavelet (scaling function) is trimmed to match the signal length.

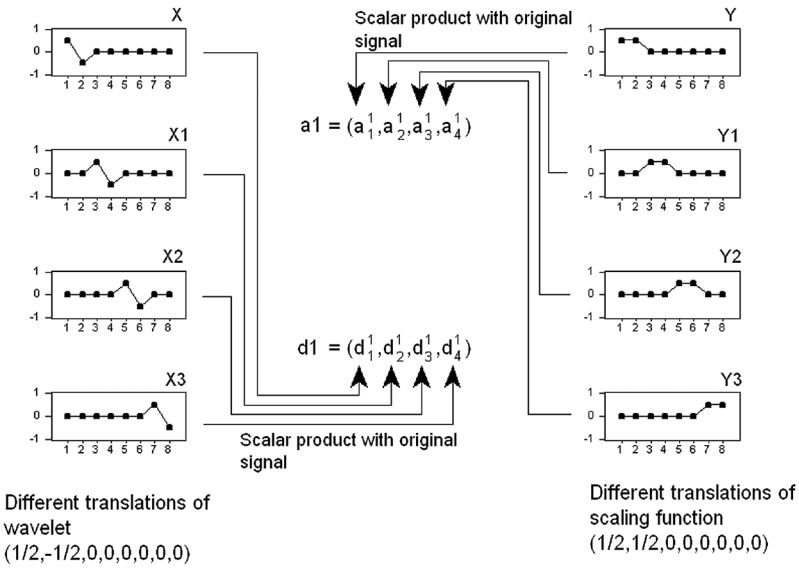

Figure 1. An illustration showing how the signal's local fluctuation (or trend) characteristics can be measured by shifting the wavelet (or the scaling function) horizontally within the signal length. Here the shifting is made at a step of the power of two.

Once the decomposition is complete, all the averaged and detail signals of different levels can be found by reconstruction. Unlike the method Walker (1999) and Fugal (2007) describe, our approach to reconstruction requires minimum mathematics. We simply reverse the procedure of decomposition, keeping only the coefficients of interest (e.g., values in box 1) and setting other coefficients to zero (*www.ag.ndsu.nodak.edu/streeter/Range_research_index.htm*). (This is explained in more detail at *www.ag.ndsu.nodak.edu/streeter/wavelets/wavelets.htm,* where we present a computer program we developed for calculating the Haar, or the modified Haar, DWT.)

Wavelet transforms on a set of the drought index signals

For the PDSI data from North Dakota (table 1), we conducted a wavelet MRA similar to the eight-element sample signal shown above, but with three important differences. First, each of the PDSI signals has data points. Second, we used the Coiflet4 wavelet instead of the Haar wavelet (figure 2a; and see *www.ag.ndsu.nodak.edu/streeter/Range_research_index.htm*) because the former is well suited to capture the smooth trend of the time series (Walker 1999). Third, we used the software TimeStat for the computation. The result of the eight-level decomposition is shown in figure 3a, and the reconstruction is shown in figure 3b for the northwestern climate region.

In figure 3a, the PDSI signal for the northwestern region is decomposed into nine frequency bands, beginning from the top with the upper band, the highest frequency band $D1$. (Note that this $D1$ corresponds to the first detail signal of our artificial signal shown above.) The name "highest frequency band" suggests that the band contains rapidly changing components and a number of different frequencies. The energy content (Walker 1999) of each of the nine signals, representing nine climate regions, is defined as the sum of squares of all 1024 data points of each of the nine frequency bands (table 1).

A few important facts about DWT. First, as shown in table 1, the time resolution becomes poorer as we move from $D1$, $D2$, ..., and all the way to $A8$. This is due to the time-frequency uncertainly principle of WT (Hubbard 1998), because the frequency resolution increases within the nine frequency bands from $D1$ to $A8$. Second, there are slight overlaps between the adjacent bands (Fugal 2007, fig. 4.7-3). However, to simplify the tabulation, these overlaps are omitted in table 1. As a result, the periods (in years) in table 1 are only approximate.

Interpretations of DWT output. From table 1 it is evident that for all nine divisions, the energy contents of the decomposed frequency bands

Table 1. Energy content of the decomposed nine frequency bands of the original PDSI signal for each of the nine climate regions of North Dakota.

Region	Decomposed frequency bands and period (years) D1 (0.1–0.2)	D2 (0.5)	D3 (1)	D4 (2)	D5 (3–5)	D6 (6–10)	D7 (11–18)	D8 (19–38)	A8 (≥ 39)	Total energy
NW	2.4	3.6	7.2	9.3	29.7	7.3	22.1	15.2	3.2	6729
NC	2.0	3.0	6.2	10.9	23.4	10.6	21.3	11.8	10.7	7747
NE	2.7	3.2	6.7	12.7	22.0	13.5	23.3	9.5	6.5	7614
WC	2.5	3.7	6.8	12.5	18.8	9.5	31.8	10.1	4.2	6779
C	2.6	3.7	6.9	11.3	20.0	14.4	30.9	6.0	4.0	7314
EC	2.1	2.8	5.1	11.2	20.3	9.6	23.3	11.9	13.7	7547
SW	2.3	3.5	5.4	11.1	23.6	12.0	32.6	8.5	1.0	7037
SC	2.1	3.0	6.0	10.3	20.1	11.3	36.4	8.8	1.9	7915
SE	2.1	2.5	4.4	11.4	21.7	5.2	23.6	24.6	4.1	8595
Average	2.3	3.2	6.1	11.2	22.2	10.4	27.3	11.8	5.5	7475

C, central; EC, east-central; NC, north-central; NE, northeast; NW, northwest; PDSI, Palmer Drought Severity Index; SC, south-central; SE, southeast, SW, southwest; WC, west-central.

Note: Data are presented as percentages of the total energy of the PDSI signal in each region.

concentrate mostly in *D*5 and *D*7, corresponding to the periods of 3–5 years and 11–18 years, respectively. The period 19–38 years (corresponding to *D*8) also has a considerable contribution, but it varies from region to region, with the southeastern region having the highest percentage (24.6%; see table 1). Without exception, the lowest energy exists in the bands of *D*1 and *A*8. The *D*1's all have very low energy because they are obtained through signal synthesis using only the first fluctuation subsignal, which represents the most detailed information. The low energy in *A*8 is due to the fact that the previous decomposition stages have successively removed the major high-energy band components. It is interesting that band *D*6 (for a period of 6–10 years) accounts for a quite low percentage of the total energy of the signals for all nine climate regions of North Dakota. Of the total energy of PDSI signals from June 1921 to September 2006, the northwestern region had the lowest value, and the southeastern region had the highest value. This indicates that there are more cases of extreme PDSI values for the southeastern part of the state than for the northwestern part.

In figure 3b, beginning from *A*8, more and more details are added to produce the original signal *f*. Signal *A*6 in figure 3b looks similar to signal *D*7 in figure 3a. That is because signal *A*7 in figure 3b has low energy, and when it is added to signal *D*7, only slight changes are made. Inspecting the stages of the signal reconstruction in figure 3b, we can see that the biggest change in the shapes of the curves occur when *A*5 is added to *D*5 to produce *A*4. This is understandable because in figure 3a, *D*5 has the highest energy of all the decomposed bands (table 1). Also, a big change in the shapes of the curves occurs when *A*7 is added to *D*7 to produce *A*6, because *D*7 has the second highest energy of the nine frequency bands of the signal from the northwestern region.

Looking at the *A*8 column in table 1, values from the southwestern and south-central regions have low energy (1.0 and 1.9, respectively), whereas the north-central and east-central regions have high energy (10.7 and 13.7, respectively). This low energy or high energy in the eighth averaged signal is consistent with the near zero long-term trend of the

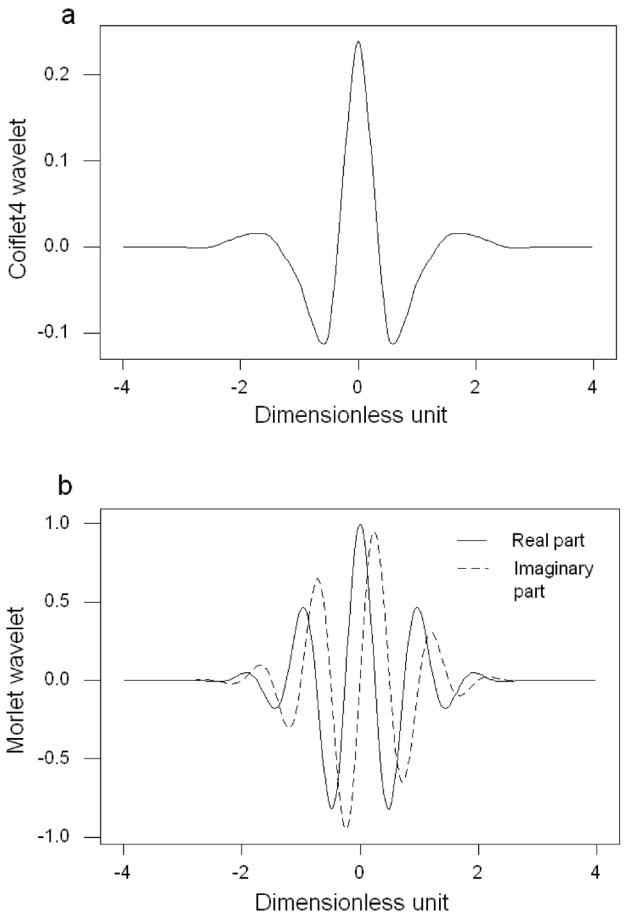

Figure 2. Shapes of the two wavelets bases used for analyzing the Palmer Drought Severity Index data in this study: (a) the Coiflet4 wavelet and (b) the Morlet wavelet.

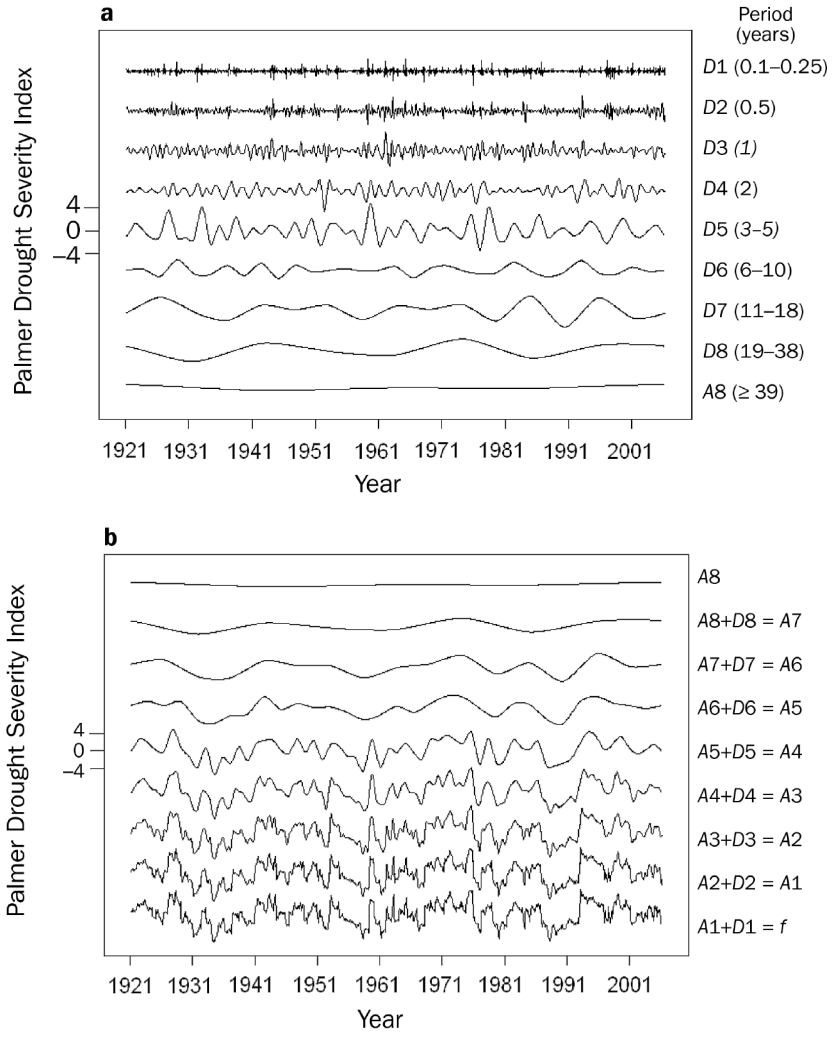

Figure 3. A decomposition and lossless reconstruction of the Palmer Drought Severity Index values for the northwestern climate region of North Dakota (June 1921–September 2006). The Coiflet4 wavelet was used for the discrete wavelet transform. (a) The original signal was subjected to eight level decompositions, resulting in the first detail signal* D*1, second detail signal* D*2,..., eighth detail* D*8 and averaged* A*8 signals. (b) The component signals were synthesized successively to obtain a perfect reconstruction of the original signal* f*. The averaged signals* A*6 and* A*8 are plotted along with the original signal in figure 4.

PDSI data in the southwestern and south-central regions and the first down, then up, trend in the north-central and east-central regions (figure 4). In figure 4, the decadal droughts of the 1930s and 1980s are clearly shown. Several regions clearly show a drought in the 1950s (especially the northwestern, north-central, west-central, and south-central regions), but overall this 1950s drought is not as strong as the droughts of 1930s and 1980s.

A time-frequency portrait of the PDSI data using CWT. Like the DWT (i.e., Haar and Coiflet4), a CWT also captures (localizes) the signal features in both time and frequency (scale) domains (Polikar 2001). However, CWT usually shows more transient features of the signals, because both the shifting and stretching of the wavelets are done at very fine intervals. Walker (1999) and Fugal (2007) presented detailed computer algorithms. Different wavelet bases can be used, such as Haar, DaubJ, CoifletI, Mexican Hat, or Morlet. In this application, we used the Morlet analytic wavelet base as shown in figure 2b. The use of the real and complex parts of the Morlet wavelet is necessary for the signal synthesis (Gould and Tobochnik 1996).

Now we turn to the CWT graphs for the northwestern and south-central regions shown in figure 5 (graphs of the other seven regions are not shown because of space limitations). The vertical axis represents the period (inverse of frequency) and the horizontal is for time (in years), so these are a time-frequency portrait of the signals. The orange and red colors in figure 5 indicate high coefficients of CWT at a particular frequency and time location. The smaller coefficients are represented by yellow or blue. The very high frequency components are located in the lower portion of the graphs in shades of blue, indicating lower energies. As with DWT, there is a trade-off between the resolution of time and frequency in a typical CWT graph (Polikar 2001). At the lower portion of the graph, the time resolution is high and the frequency resolution becomes low. At the uppermost portion of the graphs, however, the orange-colored contours tend to be horizontally wide and vertically narrow, indicating a lower time resolution but higher frequency resolution.

There are several important features in figure 5. First, for both regions (actually, for all nine regions), the droughts of the 1930s and 1980s are represented with the orange-red contours on the upper portions of the graphs. However, the 1930s drought is on the uppermost edge, corresponding to a period more than 20 years, whereas the 1980s drought is located at about the 12-year period; the droughts occurred at different time scales, with the 1930s drought lasting longer. The deepness of the orange color does not correspond to the severity of drought, but instead indicates frequencies with high energy. At scales of 10 to 20 years, no prolonged and severe drought occurred from the late 1950s to the early 1970s, as indicated by the domination of blue colors. The higher energy of the high frequency signal components occur mainly during the major droughts of the 1930s and the 1980s. In the CWT graphs, they appear as isolated, yellow-orange contours, smaller in area, below the two major droughts. In particular,

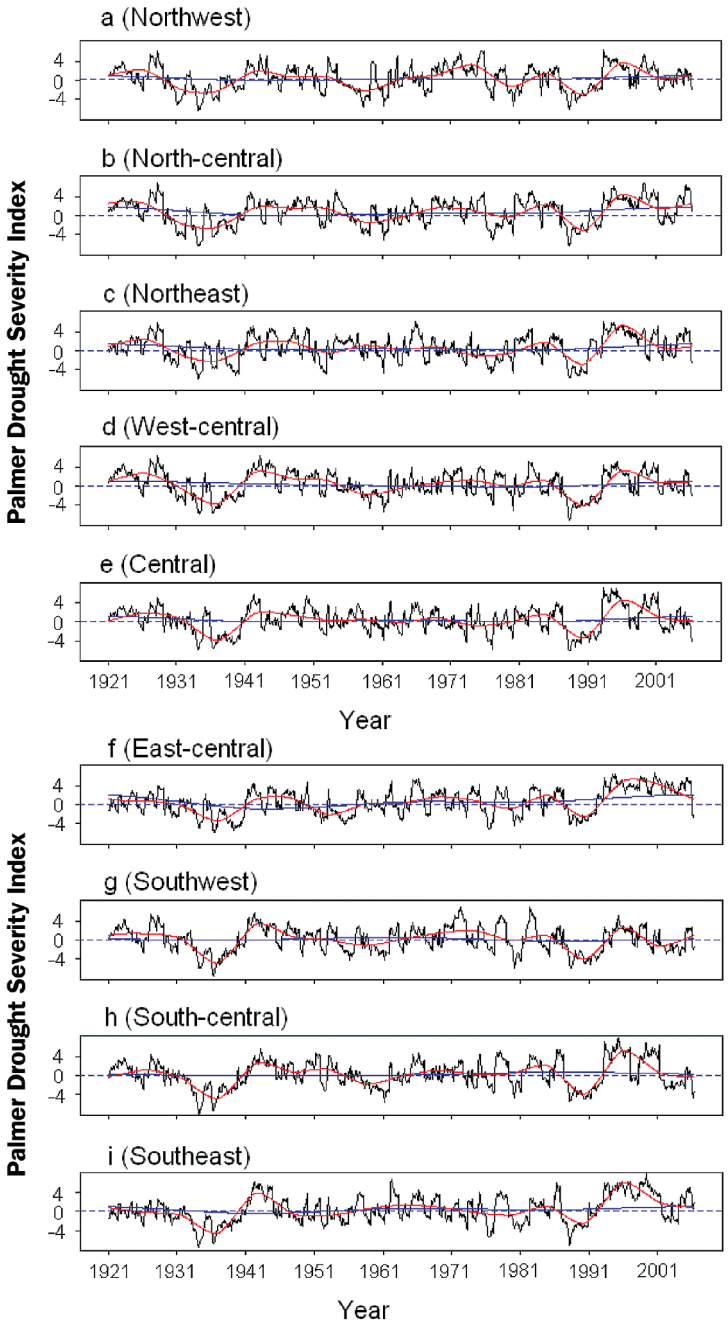

Figure 4. The Palmer Drought Severity Index and discrete wavelet transform (Coiflet4) for the nine climate regions of North Dakota with the original signal f *(solid black), the sixth averaged signal* A6 *(solid red), and the eighth average signal* A8 *(solid blue). The dashed blue lines indicate the horizontal zero.*

for the south-central region, the lack of higher frequency dynamics below the 1930s drought means that within this major drought period, the higher frequency changes of the precipitation were lacking; the drought was truly severe, with no significant temporal rain inputs. On the other hand, for the northwestern region during both the 1930s and the 1980s droughts, there are scattered higher frequency dynamics, which may have provided partial and temporal relief from the prolonged droughts.

Discussion of the PDSI data analysis. The long-term drought cycles on the earth's surface in general and in the northern Great Plains in particular is highly complex (Schubert et al. 2004a). For the major part of the Great Plains, the strongest influence of the long-term drought cycles comes from the Pacific and Atlantic sea surface temperatures (McCabe et al. 2004, Schubert et al. 2004b), solar activities (Yu and Ito 1999), and long-term soil moisture feedback, as well as possible effects of global warming (Schubert et al. 2004a). Although long-term ocean temperature trends seem to suggest that the Great Plains region is, at present, in the early stage of a long-term drought period (McCabe et al. 2004), effects of multiple influences occurring over different time scales create difficulties for accurate long-term forecasting. There are other possibilities for wavelet-based time series forecasting (Murtagh and Aussem 1998, Yin and Zheng 2004), but these are beyond the scope of this article. However, using wavelet tools (DWT and CWT), we identified several important features of the drought severity history in North Dakota. For example, using wavelet MRA, we found that the drought severity in the state for the past 85 years was dominated by a multiyear periodicity of 3 to 5 years and a decadal periodicity of 11 to 18 years. However, the 6- to 10-year period is very weak. This finding may have some implications for agriculture. Yet it was the CWT analysis that revealed the two major droughts of the 20th century (the 1930s and the 1980s droughts) and their characteristics in different areas of this state, as well as several more detailed high frequency features of the drought periodicities.

Further study and applications of wavelets

Many real-world data sets in this information-technology era can be so complex that a preliminary application of the wavelet technique is usually far from enough. We now offer a few directions for further applications of wavelets, as well as a couple of ideas with potential impacts for new developments in biology.

Wavelets in high dimensions: The basic principle unchanged. Equipped with the basic principle of wavelet MRA in one dimension, one can easily understand and use WT in higher dimensions (Walker 1999, Walker and Chen 2000), as done with the two-dimensional image shown in Strand and colleagues (2006).

Fourier transform: Toward advanced use of wavelets. As numerous studies cited in this article demonstrate, WT often outperforms Fourier transform in characterizing biological

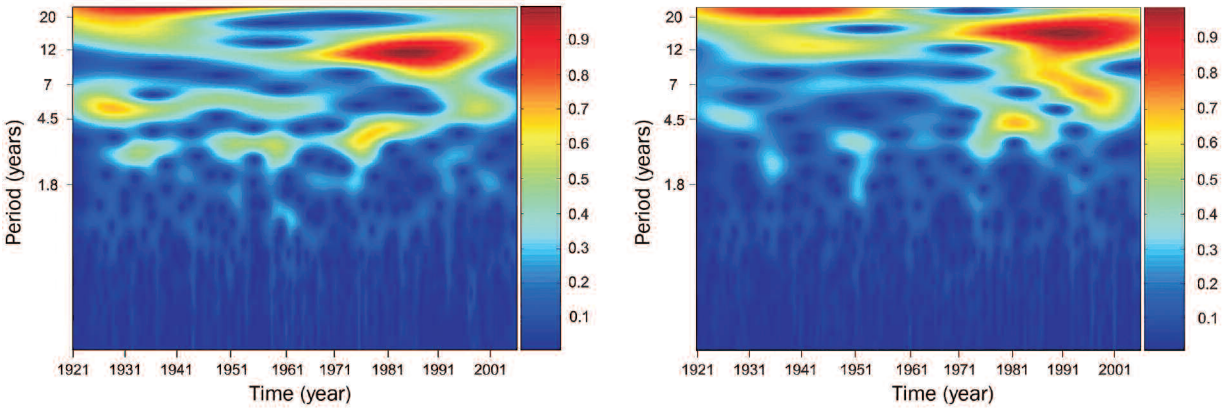

Figure 5. A continuous wavelet transform of the Palmer Drought Severity Index values for the northwestern and south-central regions of North Dakota from June 1921 to September 2006. Left: northwestern region; right: south-central region. The graphs were generated with Fraclab using a Morlet analytic wavelet of size 8. Other parameters used are f_{min} (minimum frequency) = 2–6; f_{max} (maximum frequency) = 0.5; voices = 256. The values of the wavelet coefficients are indicated in the vertical bar on the right in each graph.

signals, though one should note that they are equivalent theoretically (Bruns 2004). Advanced applications of the wavelet technique should be made on the basis of a better knowledge of the theory of DSP (Smith 1997, Walker 1999, Fugal 2007), especially that of Fourier transform.

Wavelet regression: Scale-specific biostatistics. When complex biological signals are broken down into scale-specific components through DWT, it is possible to conduct traditional regression analyses directly on the transformed (simplified) data. This may significantly improve the quality and efficiency of scientific data analysis and provide new insights that may not be obtainable if the analysis is applied on the original, and usually more complex, data (Keitt and Urban 2005, Keitt and Fischer 2006). Also rewarding are the wavelet-based statistical inferences (Torrence and Compo 1998, Mi et al. 2005).

Wavelet and nonlinear time series forecasting. When the slow-changing components of a time series are separated from the fast-changing ones using DWT, it is possible to make forecasts on the basis of multivariate analysis (Murtagh and Aussem 1998). Alternatively, if the component time series meets certain chaos criteria, some nonlinear dynamic methods may be used for scale-specific forecasting (Yin and Zheng 2004). However, we did not cover the issue of forecasting in our discussion of the PDSI data because doing so would require additional tests for the Lyapunov exponent (Baker and Gollub 1996).

DNA walks and neutral landscapes: From bioinformatics to ecology. The prominent features of a complex ecological landscape can be generated using a fairly simple wavelet-based "neutral landscape" (Keitt 2000). This technique may also have some heuristic value in genome function studies, because similar patterns exist in the DNA sequence at short- and long-range scales—that is, the "DNA walks" (Lió 2003, Haimovich et al. 2006).

Wavelet zerotrees: Toward the understanding of biological hierarchy. We propose an analogy between (a) the detection of biologically functional DNA nucleotide sequences that are interspersed in a background sequence of noncoding DNA (Haimovich et al. 2006) and (b) the extraction of the most significant wavelet coefficients determining the key features of an image (such as Lena or House, available at *http://decsai.ugr.es/~javier/denoise/test_images/index.htm*) that are interspersed in a background sequence of insignificant coefficients (Shapiro 1993). The success of the latter is attributable to the idea of a "lack of information" (Hubbard 1998) in a large number of insignificant coefficients forming treelike structures that can all be set to zero to tremendously increase the efficiency of computer encoding of images (Shapiro 1993, Walker and Chen 2000). In addition, the existence of these "zerotrees" in the images of Lena and House enables efficient image recognition: anyone seeing the Lena image will recognize the displayed object instantly, but it could take several seconds to find the particular object of interest on the page of an *I Spy* book, which does not have as many well-formed zerotrees as does the image of Lena (e.g., Lena's shoulder; *http://decsai.ugr.es/~javier/denoise/test_images/index.htm*).

Although wavelet-based analysis has already significantly expanded human understanding of DNA sequences (Arneodo et al. 1996, Audit et al. 2001, Haimovich et al. 2006), wavelet zerotrees offer a fresh angle for looking at DNA fractal landscapes. For instance, the prevalence of the noncoding zones might facilitate efficient encoding of the extraordinarily complex DNA sequences within biological cells, allowing navigation through multiple scales for enhanced communications between DNA and its environment. Moreover, the noncoding zones that facilitate the bending and looping of

DNA in higher dimensions (Arneodo et al. 1996) may also enhance the "image recognition" of DNA behavior by acting as wavelet zerotrees.

Acknowledgments

The authors thank Janet Patton for her kind efforts in editing the paper for both clarity and scientific strength. X. D. thanks Jiuping Jia in the Department of Economics and Management at Northwest Nationalities University, Lanzhou, China, for providing useful publications in financial engineering, and Roger A. Green in the Department of Computer and Electrical Engineering at North Dakota State University for discussions on the Fourier and wavelet transforms. We apologize to those authors whose works inspired us but are not cited in this article simply because of space limitations. Finally, we thank the anonymous reviewers for comments that greatly improved the manuscript.

References cited

Arneodo A, d'Aubenton-Carafa Y, Bacry E, Graves PV, Muzy JF, Thermes C. 1996. Wavelet based fractal analysis of DNA sequences. Physica D. 96: 291–320.

Audit B, Thermes C, Vaillant C, d'Aubenton-Carafa Y, Muzy JF, Arneodo A. 2001. Long-range correlations in genomic DNA: A signature of the nucleosomal structure. Physical Review Letters 86: 2471–2474.

Baker GL, Gollub JP. 1996. Chaotic Dynamics: An Introduction. 2nd ed. Cambridge (United Kingdom): Cambridge University Press.

Bradshaw GA, Spies TA. 1992. Characterizing canopy gap structure in forests using wavelet analysis. Journal of Ecology 80: 205–215.

Bruns A. 2004. Fourier-, Hilbert- and wavelet-based signal processing: Are they really different approaches? Journal of Neuroscience Methods 137: 321–332.

Csillag F, Kabos S. 2002. Wavelets, boundaries, and the spatial analysis of landscape pattern. Écoscience 9: 177–190.

Dale MRT, Mah M. 1998. The use of wavelets for spatial pattern analysis in ecology. Journal of Vegetation Science 9: 805–814.

Fugal DL. 2007. Conceptual Wavelets in Digital Signal Processing. Spring Valley (CA): Space and Signals Technologies LLC. (7 March 2008; *www.conceptualwavelets.com/index.html*)

Gould H, Tobochnik J. 1996. An Introduction to Computer Simulation Methods: Applications to Physical Systems. 2nd ed. Reading (MA): Addison-Wesley.

Haimovich AD, Byrne B, Ramaswamy R, Welsh WJ. 2006. Wavelet analysis of DNA walks. Journal of Computational Biology 13: 1289–1298.

Hubbard BB. 1998. The World According to Wavelets: The Mathematical Technique in the Making. 2nd ed. Natick (MA): A. K. Peters.

Jensen A, Cour-Harbo AL. 2000. Ripples in Mathematics: The Discrete Wavelet Transform. Berlin: Springer.

Keil A, Stolarova M, Heim S, Gruber T, Müller MM. 2003. Temporary stability of high-frequency brain oscillations in the human EEG. Brain Topography 16: 101–110.

Keitt TH. 2000. Spectral representation of neutral landscapes. Landscape Ecology 15: 479–493.

Keitt TH, Fischer J. 2006. Detection of scale-specific community dynamics using wavelets. Ecology 87: 2895–2904.

Keitt TH, Urban DL. 2005. Scale-specific inference using wavelets. Ecology 86: 2497–2504.

Lark RM, Webster R. 1999. Analysis and elucidation of soil variation using wavelets. European Journal of Soil Science 50: 185–206.

Lau K-M, Weng H. 1995. Climate signal detection using wavelet transform: How to make a time series sing. Bulletin of the American Meteorological Society 76: 2391–2402.

Lió P. 2003. Wavelets in bioinformatics and computational biology: State of art and perspective. Bioinformatics Review 19: 2–9.

[LUSCD] Locations of US Climate Divisions. 2007. (7 March 2008; *www.cdc.noaa.gov/usclimate/map.html*)

McCabe GJ, Palecki MA, Betancourt JL. 2004. Pacific and Atlantic Ocean influences on multidecadal drought frequency in the United States. Proceedings of the National Academy of Sciences 101: 4136–4141.

Mi X, Ren H, Ouyang Z, Wei W, Ma K. 2005. The use of the Mexican Hat and the Morlet wavelets for detection of ecological patterns. Plant Ecology 179: 1–19.

Murtagh F, Aussem A. 1998. Using the wavelet transform for multivariate data analysis and time series forecasting. Pages 617–624 in Hayashi C, Bock HH, Yajima K, Tanaka Y, Ohsumi N, Baba Y, eds. Data Science, Classification, and Related Methods. New York: Springer.

[NESDIS] National Environmental Satellite, Data and Information Service. 2006. (7 March 2008; *www.ncdc.noaa.gov/oa/climate/onlineprod/drought/xmgr. html*)

Polikar R. 2001. The Engineer's Ultimate Guide to Wavelet Analysis: The Wavelet Tutorial. (7 March 2008; *http://users.rowan.edu/~polikar/WAVELETS/WTtutorial.html*)

Schubert SD, Suarez MJ, Pegion PJ, Koster RD, Bacmeister JT. 2004a. Causes of long-term drought in the U.S. Great Plains. Journal of Climate 17: 485–503.

———. 2004b. On the cause of the 1930s Dust Bowl. Science 303: 1855–1859.

Selin A, Turunen J, Tanttu JT. 2007. Wavelets in recognition of bird sounds. EURASIP Journal on Advances of Signal Processing 2007. doi:1155/2007/51806

Shapiro JM. 1993. Embedded image coding using zerotrees of wavelet coefficients. IEEE Transactions on Signal Processing 41: 3445–3462.

Smith SW. 1997. The Scientist and Engineer's Guide to Digital Signal Processing. San Diego: California Technical Publishing.

Strand EK, Smith AMS, Bunting SC, Vierling LA, Hann DB, Gessler PE. 2006. Wavelet estimation of plant spatial patterns in multitemporal aerial photography. International Journal of Remote Sensing 27: 2049–2054.

Torrence C, Compo GP. 1998. A practical guide to wavelet analysis. Bulletin of the American Meteorological Society 79: 61–68.

Walker JS. 1999. A Primer on Wavelets and Their Scientific Applications. 1st ed. Boca Raton (FL): CRC Press.

Walker JS, Chen Y. 2000. Image denoising using tree-based wavelet subband correlations and shrinkage. Optical Engineering 39: 2900–2908.

Yin G, Zheng P. 2004. Forecasting stock market using wavelet theory. System Engineering: Theory, Methodology and Applications 13: 543–547.

Yu Z, Ito E. 1999. Possible solar forcing of century-scale drought frequency in the Northern Great Plains. Geology 27: 263–266.

doi:10.1641/B580512
Include this information when citing this material.